Thin Solid Films 827 (2025) 140776

Contents lists available at ScienceDirect

Thin Solid Films

journal homepage: www.elsevier.com/locate/tsf

Phase Control of Single-Crystalline Cobalt Oxide Thin Films Grown by Pulsed Laser Deposition

Maximilian Mihm *, Christian Holzmann, Johannes Seyd, Aladin Ullrich, Helmut Karl, Manfred Albrecht

Institute of Physics, University of Augsburg, Universitätsstraße 1, Augsburg, 86159, Germany

ARTICLE INFO

Keywords:
Phase control
Pulsed laser deposition
Thin film
Cobalt oxide

ABSTRACT

Functional oxides are highly fascinating materials driving much research in chemistry, physics, and materials science. In this study, we have epitaxially grown CoO and Co_3O_4 thin films on $SrTiO_3$(001) and MgO(001) substrates by pulsed laser deposition. By choosing the right deposition parameters such as substrate temperature and oxygen partial pressure, we are able to control the oxide phase and therefore the oxidation state of the transition metal controlling its physical properties. Structural analysis revealed a cube-on-cube orientation for both oxide phases with respect to the substrates and confirmed that all grown films are single-phase and single-crystalline. In addition, post-annealing in oxygen atmosphere allows to change the cobalt oxide phase from CoO to Co_3O_4. Furthermore, magnetic measurements indicated a Néel temperature of about 45 K for Co_3O_4 thin films which is close to the reported bulk value.

1. Introduction

Transition metal oxides have been studied in various forms for their interesting magnetic, optical, and electrical properties [1–6]. One of these transition metal oxides is cobalt oxide. Cobalt oxide forms two stable phases, CoO and Co_3O_4. In Co_3O_4, cobalt has two different oxidation states, Co^{2+} and Co^{3+}, while only Co^{2+} is present in CoO. Both oxides crystallize in a cubic structure: CoO crystallizes in the NaCl structure with a lattice constant of $a = 0.426$ nm, and Co_3O_4 is a spinel with a lattice constant of $a = 0.808$ nm. Magnetically, both materials show antiferromagnetic order [7,8], where CoO and Co_3O_4 have a Néel temperature of 290 K [7,9] and 40 K [10,11], respectively. They have been studied for their possible applications, like gas sensors [12], battery materials [13–15], and supercapacitors [16–18]. Furthermore, there were theoretical predictions of the linear magnetoelectric effect in A-site collinear antiferromagnetic spinel oxides [19]. This was later confirmed by experiments in bulk Co_3O_4 [8].

Cobalt oxide thin films have been prepared using different deposition techniques like RF sputtering [20,21], sol–gel process [22], chemical vapor deposition (CVD) [23–27], spray pyrolysis [28,29], atomic layer deposition (ALD) [30], ion beam sputtering (IBS) [31], spin-coating [32], and pulsed laser deposition (PLD) [33–35]. In this regard, single-crystalline films of Co_3O_4 have been achieved on different substrates like $SrTiO_3$(001) (STO) [23,30], $LaAlO_3$(001) [23], Si(001) [31], α-Al_2O_3(001) [30,34], and MgO(001) [24,30,35], while films grown on glass were polycrystalline [25,27].

In this study, we demonstrate the phase control of single-crystalline cobalt oxide thin films grown by PLD using a Co_3O_4 target. By changing either the substrate temperature or the oxygen partial pressure, we have epitaxially grown CoO and Co_3O_4 thin films on STO(001) and MgO(001) substrates with film thicknesses between 4 and 71 nm. Furthermore, with post-annealing in oxygen atmosphere, it is possible to change the phase from CoO to Co_3O_4.

Thin film deposition was performed using a PLD setup. The laser used in the setup was a Coherent ComPEX 205F system with a wavelength of 248 nm, applying a laser pulse with a repetition rate of 3 Hz and a pulse duration of 30 ns. For all films, the laser energy was 550 mJ, the fluence was 8 J/cm^2, and the number of laser pulses was 15,000 [36]. All films were deposited using a commercial Co_3O_4 target (g-Materials e. K.). Please note that typically CoO or pure Co targets were utilized in comparable studies [33–35]. We used two different substrates, STO(001) and MgO(001). The STO substrates were annealed before deposition. The annealing temperature was set to 900 °C, which was held for 3 h in ambient conditions. The annealing process leads to an atomically stepped surface, which is SrO-terminated [37]. For cobalt oxide films grown on STO(001) and MgO(001) either the substrate temperature was varied (500–650 °C) while keeping the oxygen

* Corresponding author.
E-mail address: maximilian.mihm@physik.uni-augsburg.de (M. Mihm).

https://doi.org/10.1016/j.tsf.2025.140776
Received 27 May 2025; Received in revised form 18 August 2025; Accepted 21 August 2025
Available online 28 August 2025

partial pressure constant, or the oxygen partial pressure was varied (1×10^{-3}–5 Pa) at a fixed substrate temperature.

X-ray diffraction (XRD) measurements, including wide-range reciprocal space mapping (RSM), were performed using a Rigaku Smartlab 9 kW with a rotating copper anode (Cu_{K_α} with a wavelength of 0.1541 nm) to determine the structure and phase formation of cobalt oxide thin films. The thickness of the films was determined by X-ray reflectrometry (XRR). The RSMs were simulated and the XRR curves were fitted using the Rigaku's SmartLab Studio II software. The film morphology and surface roughness was analyzed by atomic force microscopy (AFM), and images were recorded using a Dimension Icon AFM from Bruker. Zero-field-cooled (ZFC) and field-cooled (FC) measurements were performed using a superconducting quantum interference device-vibrating sample magnetometer (SQUID-VSM MPMS3, Quantum Design GmbH) to determine the magnetic order temperature of Co_3O_4 on STO(001).

2. Results and discussion

2.1. Cobalt oxide thin films on $SrTiO_3$(001)

The lattice mismatch between STO(001) and CoO(001) (−7.8%), and Co_3O_4(001) (−9.4 %) is quite large. This can be an issue when it comes to epitaxial growth. During the growth process, the substrate temperature for all following cobalt oxide films was 500 °C. Only the oxygen partial pressure was varied between 1×10^{-3} Pa and 5 Pa. Fig. 1(a) shows the 2θ scans of four different cobalt oxide films grown on STO(001) at different oxygen partial pressures. It is visible that for a low oxygen partial pressure between 1×10^{-3} Pa and 2×10^{-2} Pa, CoO is favored as indicated by the presence of the (002) reflection. The film grown at 2×10^{-2} Pa even shows Laue oscillations, which indicates smooth interfaces between substrate, film and surface and also confirms good film crystallinity. At higher oxygen partial pressure (≥0.5 Pa) Co_3O_4 is formed, as revealed by the presence of the (004) reflection. Fig. 1(b) shows the corresponding in-plane (ip) XRD scans. For the two Co_3O_4 films the expected (220) and (440) reflections are visible, while for CoO films only the (220) peak is present, because the (110) reflection is forbidden. A similar behavior in the phase formation has been observed by Matsuda et al. [34] for growing epitaxial cobalt oxide thin films on α-Al_2O_3 by PLD using a CoO target. They observed at lower oxygen partial pressure of 10^{-6} Pa that CoO was the preferred phase and at higher O_2 pressure of 1 Pa, the film only contained Co_3O_4 [34]. Prieto et al. [31] observed the same dependence of the cobalt oxide phase from a pure cobalt target growing thin films on silicon via IBS. Further, Laureti et al. [33] demonstrated that the oxygen partial pressure during the PLD process has a large impact on the growth of cobalt oxide on silicon using a cobalt target as well. At low oxygen partial pressure of 10^{-2} Pa, they observed just pure cobalt peaks, but after increasing the oxygen partial pressure to 1 Pa, the polycrystalline film contained both CoO and Co_3O_4 [33].

The thickness of the films was determined with XRR, two examples of XRR curves with the corresponding fits are shown in Fig. A.1. The film thicknesses are in the range between 6 and 22 nm as summarized in Table 1. The corresponding fit values can be found in the Appendix in Table A.1. Please note that the film thickness does not follow a clear trend with increasing oxygen partial pressure. The reason for that is that the window where the laser beam enters the chamber will also be coated. Therefore, the fluence gets decreased and alters the growth rate (nm/puls). Besides that the position of the substrate on the sample holder also has an influence on the growth rate. The surface roughness of all films is well below 1 nm and matches well the root mean square (RMS) roughness extracted from AFM images. A change in morphology from a stepped (CoO) to a grainy (Co_3O_4) surface is visible, see Fig. A.2.

In the 2θ scans (Fig. 1(a)), there was no peak shift visible between the films grown at 1×10^{-3} Pa O_2 and 2×10^{-2} Pa O_2; the same was observed in the ip XRD scan. However, for films grown at higher oxygen partial pressures, a slight shift of the Co_3O_4 peak is observed in the 2θ scan as well as in the ip scan. The calculated out-of-plane (oop) and ip lattice constants of the films are summarized in Table 1. Three out of the four prepared films have an oop lattice constant larger than the corresponding ip lattice constant. Only for the film grown at 5 Pa O_2 the ip lattice constant is larger. The reason for that could be, that this is the thinnest film of this series with 6 nm and with increasing thickness the film starts to relax in the oop direction. This shows that all films are slightly tetragonally distorted. The lattice constant of CoO is larger than that of STO. Also, two times the lattice constant of Co_3O_4 is larger than the lattice constant of STO (~0.781 nm). Thus, the lattice of the cobalt oxides will be under ip compressive stress which leads to an expansion in the *c*-direction and a compression in the *a*- and *b*-direction.

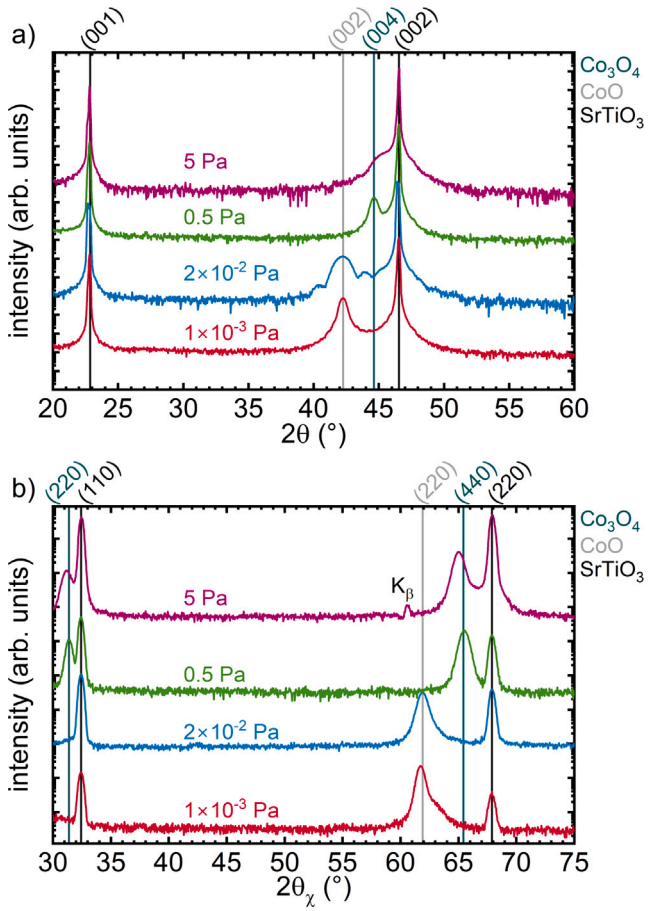

Fig. 1. XRD scans of cobalt oxide films grown on STO(001) at different oxygen partial pressures at 500 °C. (a) 2θ scan, and (b) ip XRD measurements at $\chi = 0°$.

Rocking curve measurements were performed using the (002) reflection for CoO and the (004) reflection for Co_3O_4. To extract the full width at half maximum (FWHM), we fitted the peaks using a Gaussian function. The values of the fits are given in Table 1. The 22 nm thick Co_3O_4 film grown at 500 °C with an O_2 pressure of 0.5 Pa has a FWHM of 1.219°. This value is four times larger than the FWHM which Shalini et al. [23] has reported. They used a different growth technique which could be responsible for the difference. In addition, in two films (6 nm and 8 nm) we observed a convolution of two peaks (see Fig. A.3(a)) in the rocking curves. Therefore, we performed a deconvolution to get the FWHM of both peaks. Most probably, one region in our film has a better crystal quality, which leads to the sharp peak, and another part, has a lower crystal quality which is responsible for the broader FWHM. The reason for that could be that the films are not fully relaxed as these films are the thinnest ones.

Table 1
Calculated oop (a_{oop}) and ip (a_{ip}) lattice constants for cobalt oxide thin films grown on STO(001) at a substrate temperature of 500 °C. In addition, values of the film thicknesses determined with XRR measurements, FWHM of the (002) reflection for CoO and of the (004) reflection for Co_3O_4, and phase of the cobalt oxide film are given.

O_2 pressure (Pa)	a_{oop} (nm)	a_{ip} (nm)	Thickness (nm)	FWHM (°)	Phase
1×10^{-3}	0.4276	0.4247	22	1.357	CoO
2×10^{-2}	0.4280	0.4239	8	0.172 and 2.057	CoO
0.5	0.8116	0.8056	22	1.219	Co_3O_4
5	0.7871	0.8117	6	0.169 and 1.161	Co_3O_4

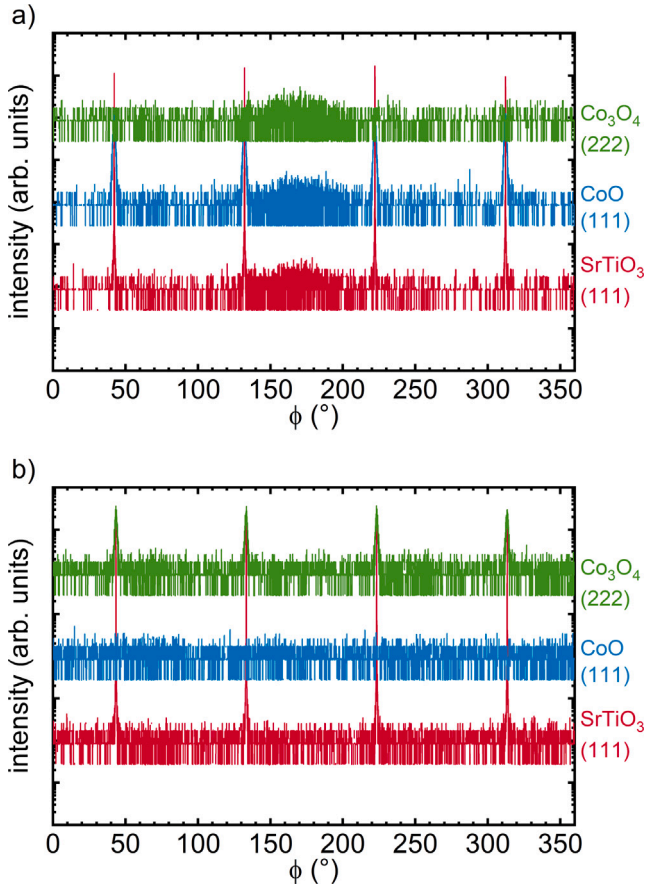

Fig. 2. ϕ scans around the (111) reflex of STO and CoO, and ϕ scan around the (222) reflex of Co_3O_4 for 22 nm thick films grown at an oxygen partial pressure of (a) 1×10^{-3} Pa, and (b) 0.5 Pa. The broad peak at 180° in (a) is most probably due to the substrate.

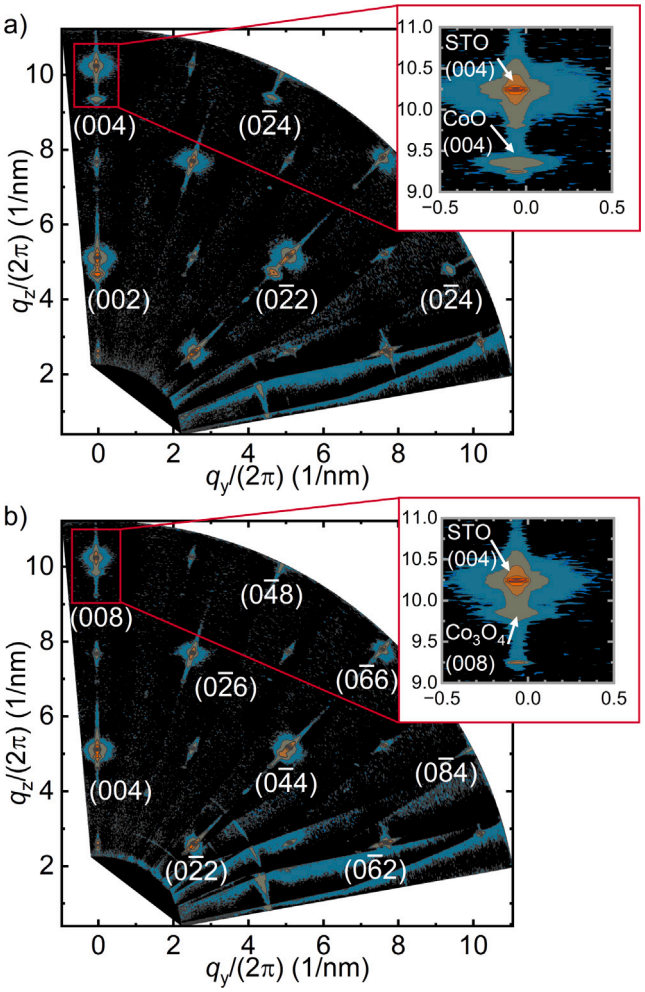

Fig. 3. Wide-range reciprocal space mapping of (a) a 22 nm thick CoO film grown at 1×10^{-3} Pa O_2 and (b) a 22 nm thick Co_3O_4 film grown at 0.5 Pa O_2 on STO(001). The enlargement shows the STO(004) reflection with the (a) CoO(004) and (b) the Co_3O_4(008) peak. The Miller indices in the RSMs mark the reflections of either the CoO or the Co_3O_4 film. Please note that the wide-range reciprocal space maps are stitched together from several pictures, which gave rise to artifacts in the picture.

To check if there is a rotation between the substrate lattice and the film lattice, ϕ scans were performed around the (111) reflection of STO and CoO, and for Co_3O_4 around the (222) reflection. Fig. 2(a) and (b) are showing the ϕ scans for the 22 nm thick films deposited at 1×10^{-3} Pa and 0.5 Pa O_2, respectively. The four peaks, which were observed in the scans, confirm the four-fold symmetry of the cubic system. There is no offset visible between the CoO and STO in Fig. 2(a). Furthermore, also in Fig. 2(b) there is no offset visible between the four STO and the four Co_3O_4 peaks. This confirms perfect cube-on-cube growth of both cobalt oxide phases on STO(001).

To confirm the observation of the ϕ scans wide-range RSM was performed. Fig. 3 shows the RSMs for both films. The substrate peaks are labeled in the RSM. For confirmation of the single-crystalline nature of the film, the theoretical peak positions of STO, CoO, and Co_3O_4 were simulated. With the simulation, all observed peaks could be reproduced (not shown), which means that we can confirm that the films are single-phase and single-crystalline. Also, the cube-on-cube growth was again confirmed by the RSM results.

In a further study, we have investigated the magnetic properties of our films using ZFC and FC curves. Fig. 4 displays the ZFC and FC curves of a 71 nm thick Co_3O_4 film grown at 550 °C at 0.5 Pa O_2 on STO(001) from 5 to 375 K with a guiding field of 100 mT. For the ZFC curve the sample was cooled down without an applied field, after reaching 5 K the guiding field was switched on, and during the heating the magnetization was measured. In the FC sequence the sample was

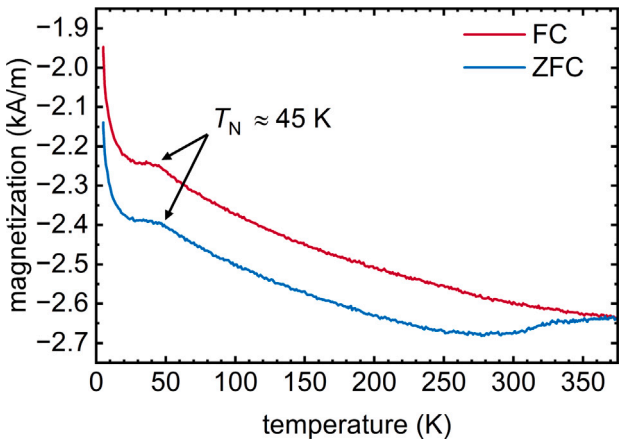

Fig. 4. Zero-field-cooled (ZFC) and field-cooled (FC) measurements of a 71 nm thick Co_3O_4 film grown on STO(001) at 550 °C and 0.5 Pa O_2.

Table 2
Cobalt oxide films grown on MgO(001) with different oxygen partial pressures at 500 °C. In addition, film thicknesses determined with XRR measurements, FWHM of the (002) reflection for CoO and phase of the cobalt oxide film are given.

O_2 pressure (Pa)	Thickness (nm)	FWHM (°)	Phase
1×10^{-3}	19	0.144 and 0.922	CoO
0.5	17	0.136 and 1.206	CoO
5	5	0.159 and 2.402	CoO

cooled down with an applied field, which had the same value as the guiding field. After reaching the temperature the magnetization was measured during the heating again with a guiding field. It is visible that with decreasing temperature, the magnetization starts to increase for the FC curve. For the ZFC the magnetization first starts to decrease and around 280 K the magnetization starts to increase. Around 45 K a kink is visible in both curves and the magnetization is nearly constant till 20 K and then starts to rise again. The position of the kink (~45 K) is in good agreement with the Néel temperature of bulk Co_3O_4 (~40 K) [7,11]. The difference could originate from the strain in the thin film and also from oxygen vacancies. Please note that the rise in magnetization below 20 K is a substrate effect, as confirmed by measurements of a blank STO substrate under the same conditions (Fig. A.4). Attempts to measure the Néel temperature of CoO failed due to the low signal.

2.2. Cobalt oxide thin films on MgO(001)

A substrate with a much smaller lattice mismatch to CoO (−1.1%) and Co_3O_4 (−2.2%) is MgO(001). This makes it a suitable substrate for epitaxial growth of both cobalt oxide phases. During the deposition of the films on STO(001), a piece of MgO(001) was simultaneously deposited to ensure the same growth conditions. Fig. 5 shows the XRD scan of cobalt oxide thin films at 500 °C with different oxygen partial pressures. All films show the (002) and (004) reflections of CoO. The films grown at 1×10^{-3} Pa and 0.5 Pa O_2 pressure show Laue oscillations. The thickness of the films, as extracted from XRR measurements, are given in Table 2. It can be observed that with increasing oxygen partial pressure the film thickness is decreasing from 19 to 5 nm. Similar surface roughness of the cobalt oxide films on MgO(001) were achieved, despite having a smaller lattice mismatch compared to STO(001), see Table A.1. All three films showed a convolution of two contributions in the rocking curve scans, examples are shown in Fig. A.3(b). The FWHM are also included in Table 2. As only CoO was observed with increasing oxygen partial pressure, we decided to keep the oxygen partial pressure constant and varied the substrate temperature.

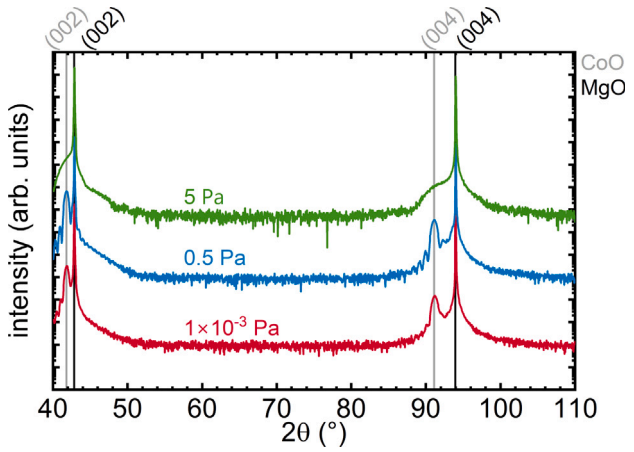

Fig. 5. 2θ scans of cobalt oxide films grown on MgO(001) with different oxygen partial pressures at 500 °C.

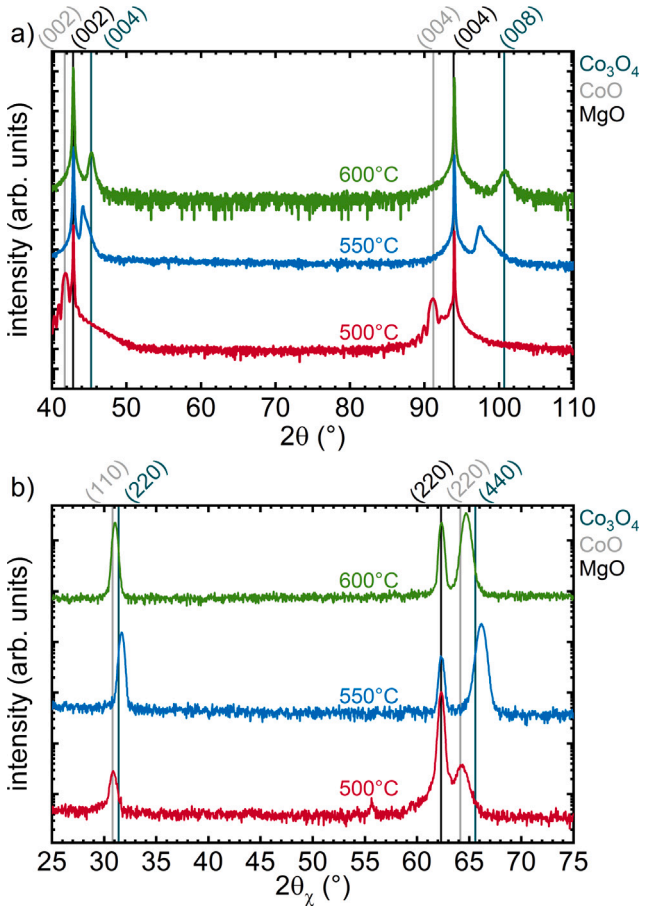

Fig. 6. XRD scans of cobalt oxide films grown on MgO(001) using different substrate temperatures and an oxygen partial pressure of 0.5 Pa. (a) 2θ scan, and (b) ip XRD measurements at $\chi = 0°$.

In Fig. 6(a), 2θ scans and (b) ip scans of three different cobalt oxide films grown on MgO(001) at different substrate temperatures are presented. The oxygen partial pressure was 0.5 Pa for all films. In Fig. 6(a) it is observed that the film peak moves from the left side to the right side of the substrate peak by increasing the substrate temperature

Table 3
Calculated oop (a_{oop}) and ip (a_{ip}) lattice constants for cobalt oxide thin films grown on MgO(001) at an oxygen partial pressure of 0.5 Pa. In addition, film thicknesses determined with X-ray reflection measurements, FWHM of the (002) reflection for CoO, and of the (004) reflection for Co_3O_4, and phase of the cobalt oxide film are given.

Substrate temperature (°C)	a_{oop} (nm)	a_{ip} (nm)	Thickness (nm)	FWHM (°)	Phase
500	0.4317	0.4131	17	0.136 and 1.206	CoO
550	0.8200	0.7980	4	0.784	Co_3O_4
600	0.8001	0.8144	35	1.070	Co_3O_4

just by 50 °C, indicating that the cobalt oxide phase changes from CoO to Co_3O_4. Laue oscillations are also visible for the 17 nm thick CoO film. Phase control of cobalt oxide films grown on MgO(001) was also previously reported using a CoO target for the PLD process and varying the oxygen partial pressure [35]. Prieto et al. [31] used IBS to grow thin films of cobalt oxide on silicon. They observed a single-phase CoO film at higher temperatures and a single-phase Co_3O_4 film at lower temperatures [31], in contrast to our observations. A reason for this could be that they used a pure cobalt target, while we used a Co_3O_4 target. It is also visible that with increasing temperature, the oop lattice constant of Co_3O_4 is getting smaller as the (008) peak shifts to larger 2θ values with increasing temperature from 550 °C to 600 °C. Fig. 6(b) shows the ip diffraction pattern of these three samples. The sample deposited at 500 °C shows the (110) and the (220) peaks of CoO. Please note that the (110) is a forbidden peak but can appear due to strain in the lattice. It is also visible that the (220) reflection shifts to higher 2θ values, which means the ip lattice constant is smaller compared to the oop constant. For the samples deposited at 550 °C and 600 °C, the peaks move to lower and higher 2θ values, respectively. The calculated lattice parameters are displayed in Table 3. All three samples on MgO(001) show a tetragonal distortion similar to the samples deposited on STO(001). For one of the samples the ip lattice constant is actually larger than the oop lattice constant. We also performed rocking curve measurements. The same reflections as for the films on STO(001) were used for CoO and Co_3O_4. The values of the FWHM are shown in Table 3. Also here we had the convolution of two contributions, but only for the 17 nm thick film grown at 500 °C. The thinnest 4 nm thick Co_3O_4 film grown at 550 °C showed the best FWHM (0.784°), which is still higher than those reported in the literature [24,30]. Fig. 7(a) displays the wide-range RSM for a CoO film grown at 500 °C and (b) for a Co_3O_4 film grown at 600 °C. Both RSMs confirm the cube-on-cube growth of CoO and Co_3O_4 on MgO(001). This means there is no rotation between film and substrate, which was also reported for other deposition techniques like metalorganic vapor deposition [24]. The peaks between the labeled substrate peaks are corresponding forbidden peaks, either from CoO, Co_3O_4, or MgO. This was confirmed with simulated RSMs (not shown). From the XRD data and RSMs we can say that all cobalt oxide films grown on MgO(001) are single-phase and single-crystalline. Attempts to measure the Néel temperature of CoO and Co_3O_4 failed due to the strong diamagnetic signal of the MgO substrate.

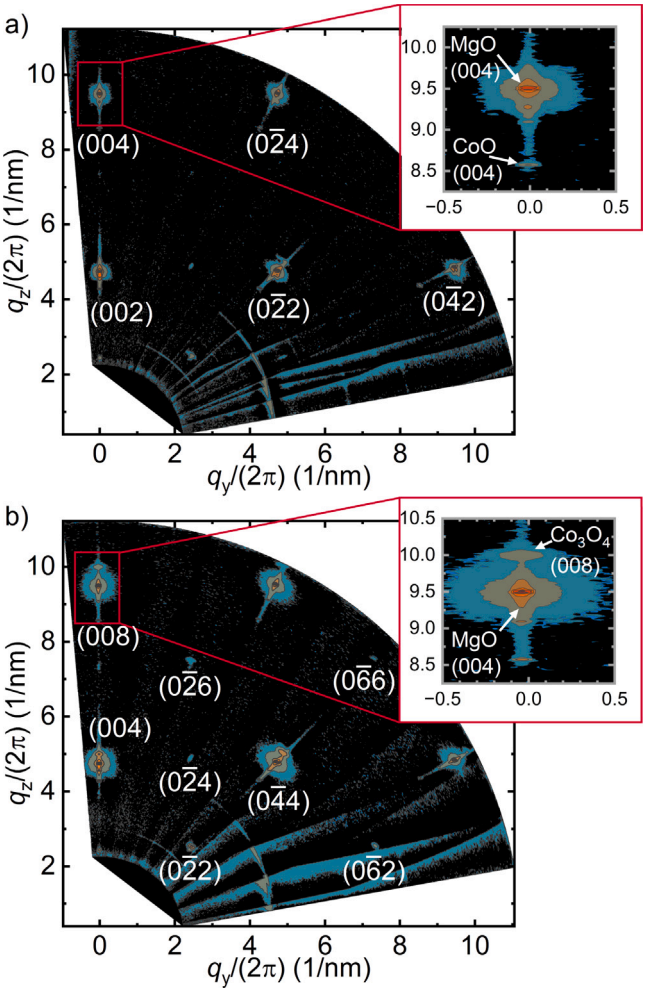

Fig. 7. Wide-range reciprocal space mapping of (a) a CoO film (grown at 500 °C) and (b) a Co_3O_4 film (grown at 600 °C) deposited on MgO(001). The inset shows the MgO(004) reflection with the (a) CoO(004) and (b) the Co_3O_4(008) peak. The Miller indices in the RSMs mark the reflections of either the CoO or the Co_3O_4 film. Please note that the wide-range reciprocal space maps are stitched together from several pictures, which gave rise to artifacts in the picture.

2.3. Annealing study

As shown before, we noticed that we can easily control the cobalt oxide phase with increasing oxygen partial pressure or substrate temperature and thus the valence state of Co. Therefore, we decided to anneal a 22 nm thick CoO film grown on STO(001) and a 19 nm thick CoO film on MgO(001) to see if the cobalt oxide phase can be changed. We annealed the samples at 900 °C for 3 h in oxygen atmosphere. The XRD scans of the as-deposited and annealed films are presented in Fig. 8(a) for STO(001) and (b) for MgO(001). Both CoO films, either grown on STO(001) or MgO(001), have changed their value of the lattice parameter as the film peak in both cases shifted to higher 2θ values. This new peak positions fit with the theoretical ones of (004) and (008) reflections of Co_3O_4. To check if the phase change is reversible, we annealed the newly formed Co_3O_4 films in vacuum ($p \sim 5 \times 10^3$ Pa) at 900 °C for 3 h. The XRD scan (not shown) revealed no change for the film grown on MgO(001), however the film on STO(001) disintegrated into a polycrystalline film. Wang et al. [38] showed that with annealing cobalt oxide in different atmospheres, the valence state of cobalt can be controlled. They have observed that in N_2 atmosphere, thin films

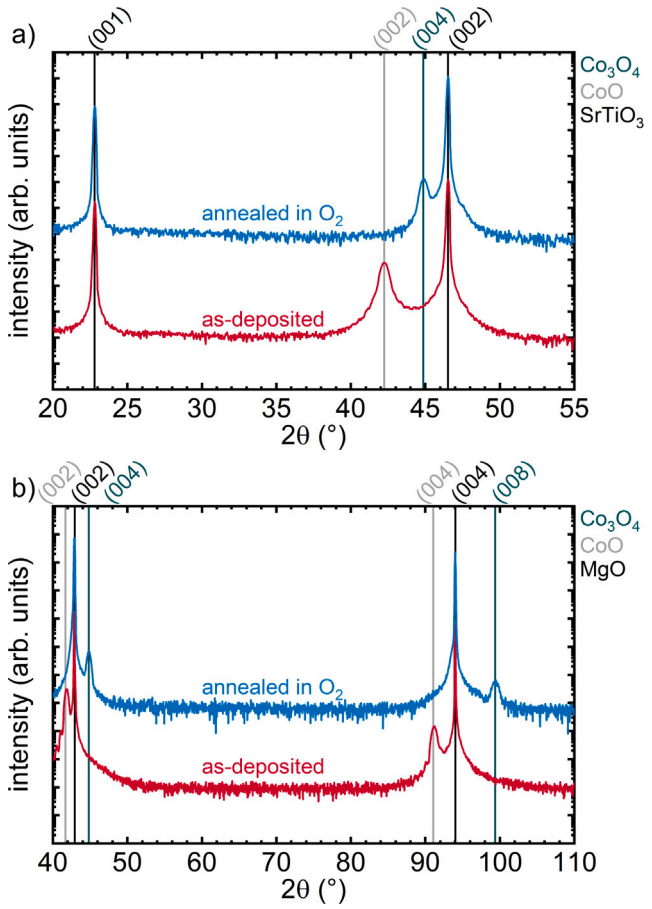

Fig. 8. XRD pattern for CoO films, annealed at 900 °C for 3 h in an oxygen atmosphere, grown on (a) STO(001), and (b) MgO(001).

of Co_3O_4 transformed into CoO between 400 °C and 600 °C. It has also been reported that bulk Co_3O_4 decomposes into CoO around 900 °C to 950 °C in air [39]. Further, Cheng et al. [27] showed that annealing bulk Co_3O_4 in vacuum (1×10^{-2} Pa) at 300 °C for 3 h leads to the formation of CoO. Nevertheless, our films did not decompose into CoO, which means the oxygen partial pressure used in our case was probably too high. Another interesting approach was reported by Kaneko et al. showing that a phase change can also be induced by vacuum ultraviolet irradiation [40].

2.4. Comparison to literature

Fig. 9 displays a phase diagram where epitaxial growth of CoO and Co_3O_4 on (a) STO(001) and (b) MgO(001) was achieved in our study. The orange area marks the Co_3O_4 region, the blue area the CoO region, and in the white area, CoO is most likely stabilized, but no data points were available here. For the growth on STO(001), a threshold value for the oxygen partial pressure is visible. Around 0.1 Pa the phase changes from CoO to Co_3O_4. While for STO(001) this change is probably constant for the whole temperature range, on MgO(001) the stabilization of Co_3O_4 occurs at temperatures higher than 500 °C. Co_3O_4 can be grown single-crystalline on STO(001) even at 5 Pa O_2 and at 600 °C (see Fig. A.5(a) and (b)). We were also able to grow single-crystalline Co_3O_4 films on STO(001) at an oxygen partial pressure of 0.5 Pa and temperature of 550 °C. The same holds true for cobalt oxide films grown on MgO(001), of which we have grown films at up to 650 °C with an oxygen partial pressure of 5 Pa. The XRD scans of these can also be found in the appendix Fig. A.6. A phase diagram summarizing results for single-crystal cobalt oxide films is presented in Fig. 9(c). Here we included results obtained by different techniques and different substrates, but they have in common that films were prepared using a CoO target, expect for mist-CVD [41]. A similar threshold for the oxygen partial pressure for PLD [34,35] and IBS [31] was observed. For IBS, a lower temperature (330 °C) and lower oxygen partial pressure ($p \sim 10^{-3}$ Pa), compared to PLD, is needed to stabilize the Co_3O_4 phase [31]. Interestingly, CoO [34,40] and Co_3O_4 [34] could even be stabilized at room temperature on α-Al_2O_3. Matsuda et al. observed a phase change from CoO to Co_3O_4 with increasing oxygen partial pressure [34]. Furthermore, Chen et al. have grown Co_3O_4 on α-Al_2O_3 using mist-CVD with a substrate temperature of 500 °C and an oxygen partial pressure of 1×10^6 Pa [41]. In addition, they decreased the substrate temperature to 450 °C and used nitrogen instead of oxygen, which resulted in the stabilization of CoO (not included in the phase diagram). Overall, the data fit perfectly to our observations, as high oxygen partial pressure results in Co_3O_4 while low oxygen partial pressure leads to the CoO phase.

3. Conclusion

In summary, we have epitaxially grown thin films of CoO and Co_3O_4 on MgO(001) and STO(001) substrates. It was shown that it is possible to control the phase of cobalt oxide by either varying the oxygen partial pressure or changing the substrate temperature. A higher oxygen partial pressure favors the growth of Co_3O_4 on STO(001). The threshold value for the phase changes is in the range from 2×10^{-2} Pa to 0.5 Pa. Furthermore, at 500 °C CoO will be stabilized on MgO(001), while Co_3O_4 is favored by increasing the substrate temperature to 550 °C. All films prepared in this work were single-phase and single-crystalline, which was confirmed by XRD and wide-range RSMs. This and further XRD measurements also revealed a perfect cube-on-cube growth of the thin films. Nevertheless, all prepared films showed a slight tetragonal distortion. By post-annealing in oxygen atmosphere, it is possible to change the phase of cobalt oxide from CoO to Co_3O_4, while post-annealing of Co_3O_4 films in vacuum did not lead to a change or even to a degradation. ZFC and FC measurements on Co_3O_4 film grown on STO(001) revealed a Néel temperature of about 45 K, which is close to the bulk value (~40 K).

CRediT authorship contribution statement

Maximilian Mihm: Writing – original draft, Investigation, Formal analysis, Conceptualization. **Christian Holzmann:** Writing – review & editing, Validation, Formal analysis. **Johannes Seyd:** Writing – review & editing, Formal analysis. **Aladin Ullrich:** Writing – review & editing, Formal analysis. **Helmut Karl:** Writing – review & editing, Formal analysis. **Manfred Albrecht:** Writing – review & editing, Supervision, Funding acquisition, Conceptualization.

Declaration of competing interest

The authors declare that they have no known competing financial interests or personal relationships that could have appeared to influence the work reported in this paper.

Acknowledgments

The authors gratefully acknowledge funding from Deutsche Forschungsgemeinschaft, Germany (DFG grant 318592081).

Appendix

See Figs. A.1–A.6 and Table A.1.

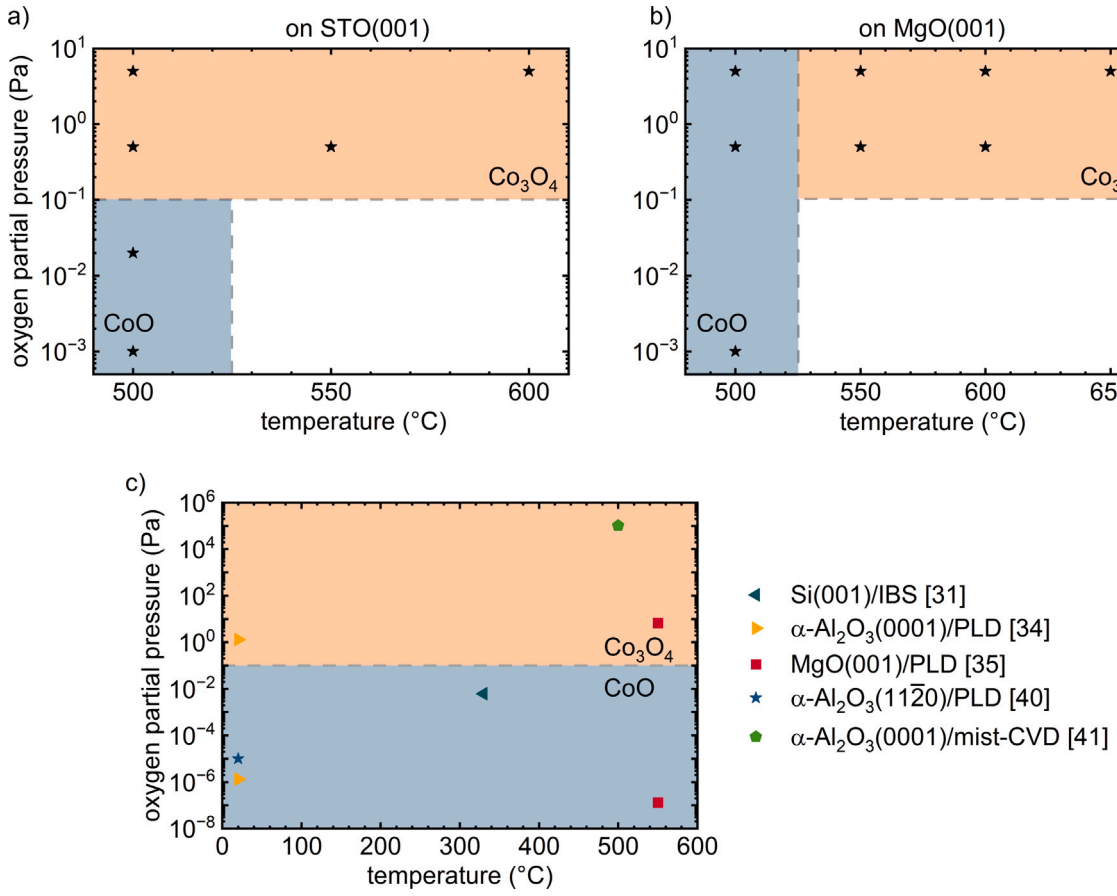

Fig. 9. Phase diagram of cobalt oxide films grown with a Co_3O_4 target on (a) STO(001), (b) on MgO(001) in our study. (c) shows the phase diagram of cobalt oxide films grown with PLD or IBS using a CoO target extracted from literature. The blue area marks where CoO is stabilized and the orange one where Co_3O_4 grows single-crystalline. In the white area in (a), (b) no data are available but CoO is most likely stabilized.

Table A.1
Fit parameters of the XRR fits for all grown cobalt oxide films. T is the substrate temperature, O_2 pressure is the oxygen partial pressure during the deposition, t_{film} is the film thickness, ρ is the density of the film or the substrate surface (sub), rgh_{film} is the roughness of the film and rgh_{sub} the roughness of the interface between substrate and film, and the R-factor describes the quality of the fit.

Substrate	Film	T (°C)	O_2 pressure (Pa)	t_{film} (nm)	ρ_{film} (g/cm^3)	ρ_{sub} (g/cm^3)	rgh_{film} (nm)	rgh_{sub} (nm)	R-factor (%)
STO(001)	CoO	500	1×10^{-3}	22	6.227	3.954	0.159	0.285	3.069
STO(001)	CoO	500	2×10^{-2}	8	6.416	4.603	0.300	0.209	1.136
STO(001)	Co_3O_4	500	0.5	22	6.250	4.753	0.203	0.238	1.439
STO(001)	Co_3O_4	550	0.5	71	5.946	5.133	0.238	1.130	6.704
STO(001)	Co_3O_4	500	5	6	5.758	4.697	0.515	0.101	3.127
STO(001)	Co_3O_4	600	5	31	6.098	4.521	0.344	0.494	1.889
MgO(001)	CoO	500	1×10^{-3}	19	6.141	3.150	0.100	0.447	2.555
MgO(001)	CoO	500	0.5	17	6.156	3.160	0.100	0.359	2.496
MgO(001)	CoO	500	5	5	3.300	1.786	0.361	0.393	1.661
MgO(001)	Co_3O_4	550	0.5	4	5.900	5.484	0.178	0.004	1.056
MgO(001)	Co_3O_4	600	0.5	35	5.939	3.584	0.272	0.954	3.675
MgO(001)	Co_3O_4	550	5	57	6.000	4.357	0.219	0.603	2.107
MgO(001)	Co_3O_4	600	5	34	5.091	2.098	0.162	0.517	2.754
MgO(001)	Co_3O_4	650	5	50	6.042	3.029	0.239	0.933	2.853

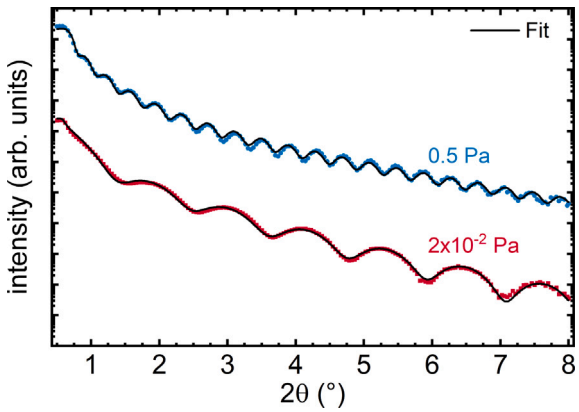

Fig. A.1. XRR measurements and fits for two cobalt oxide films grown on STO(001) with different oxygen partial pressure at 500 °C. The film grown with an oxygen partial pressure of 2×10^{-2} Pa is 8 nm thick, and the one grown with 0.5 Pa O_2 pressure is 22 nm thick (see Table A.1).

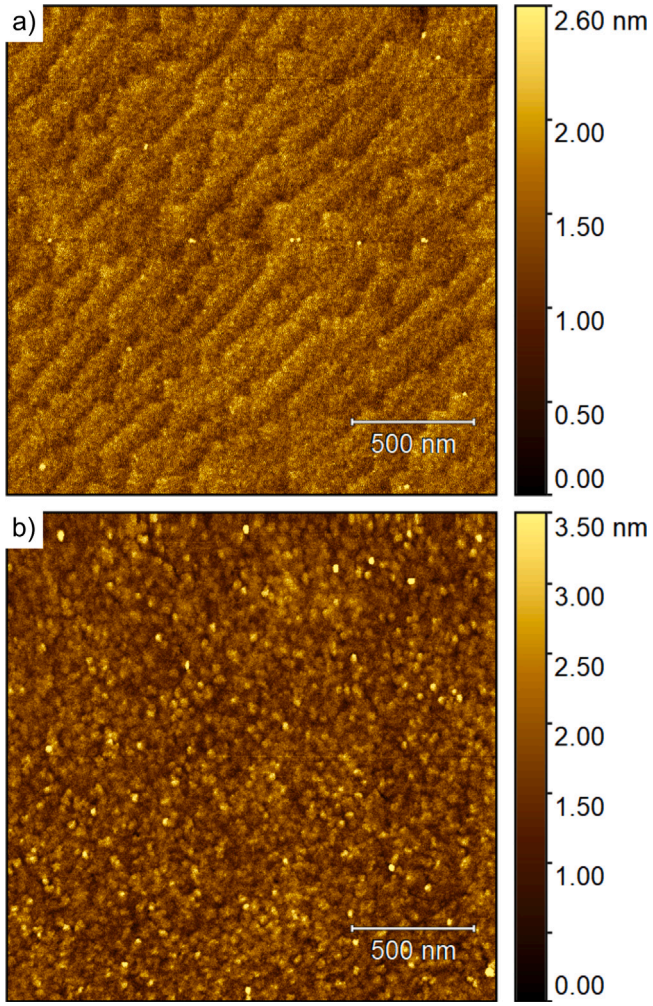

Fig. A.2. AFM images of two cobalt oxide films grown on STO(001). (a) 8 nm thick CoO film deposited at 500 °C with an oxygen partial pressure of 2×10^{-2} Pa and (b) 5 nm thick Co_3O_4 film deposited at 500 °C with an oxygen partial pressure of 5 Pa. The CoO film in (a) has a stepped surface, while the Co_3O_4 film in (b) has a grainy surface. The RMS roughness of the CoO and Co_3O_4 film is 0.36 nm and 0.46 nm, respectively.

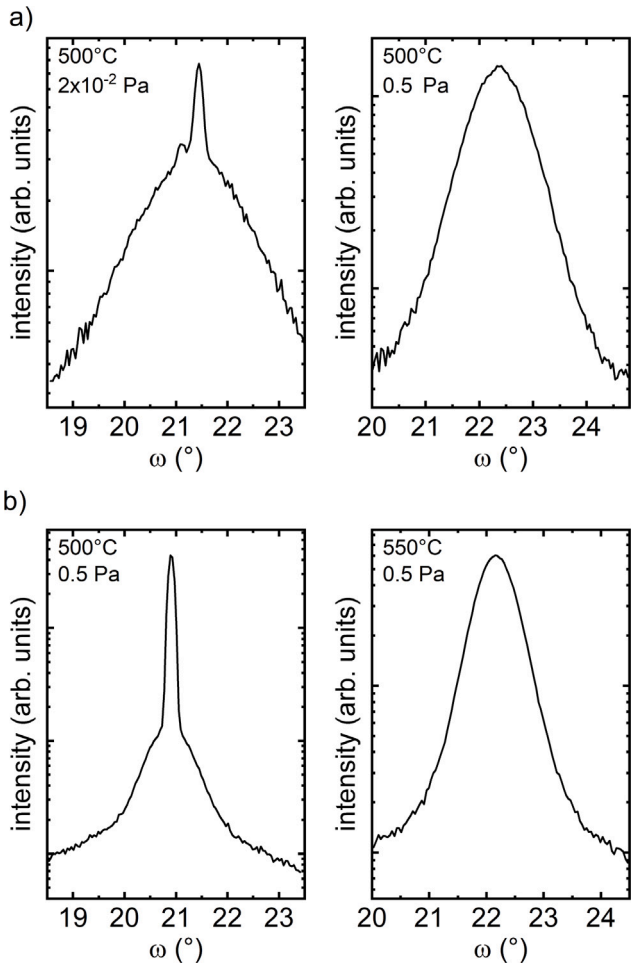

Fig. A.3. Rocking curve measurements of cobalt oxide films grown on (a) STO(001) at 500 °C, and (b) MgO(001) at 550 °C. We observed that some rocking curves showed a convolution of two reflections, while the other only consist of one.

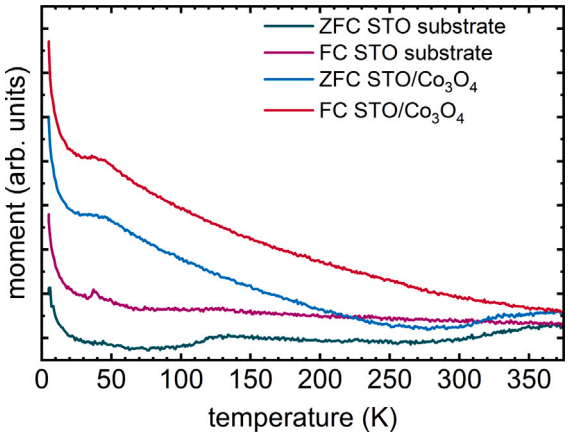

Fig. A.4. ZFC and FC measurements of an STO(001) substrate and a 71 nm thick Co_3O_4 film grown on STO(001), with a guiding field of 100 mT.

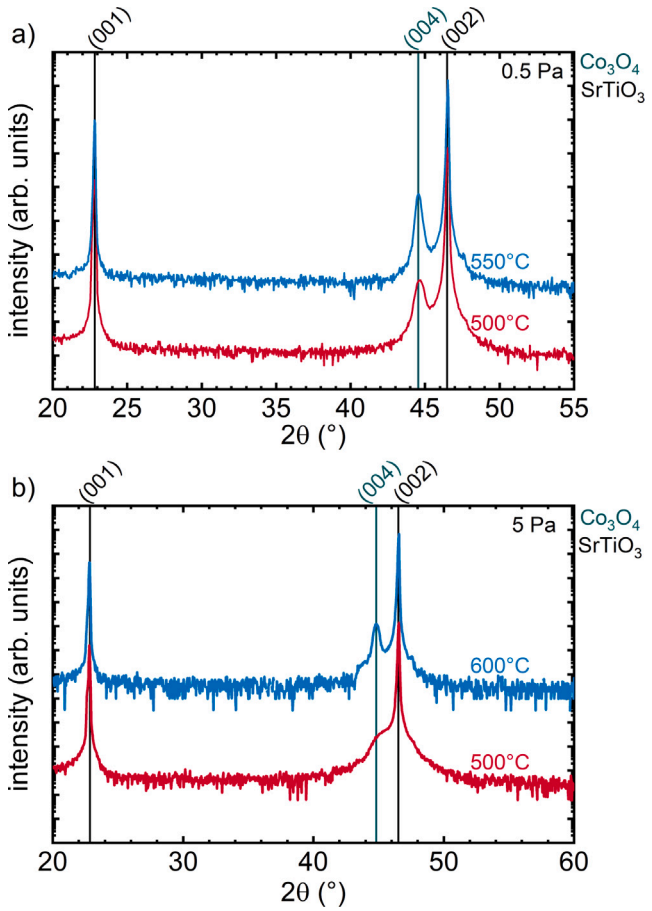

Fig. A.5. XRD scans of Co_3O_4 films grown on STO(001) (a) at 500 °C and 550 °C with an oxygen partial pressure of 0.5 Pa, and (b) at 500 °C and 600 °C with an oxygen partial pressure of 5 Pa. It is clearly visible that the cobalt oxide phase does not change with increasing oxygen partial pressure and substrate temperature. All grown films are single-phase and single-crystalline.

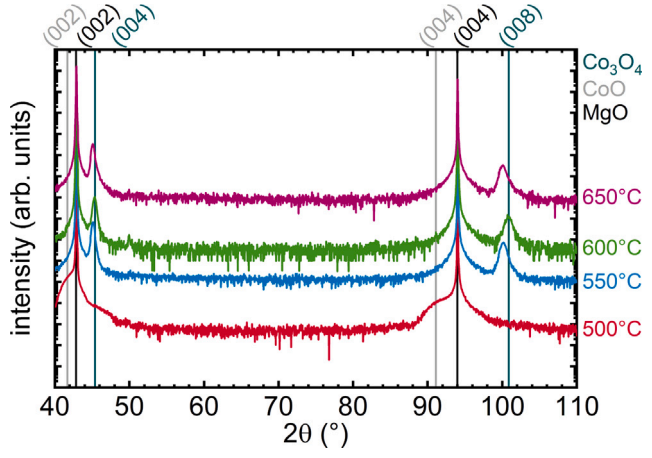

Fig. A.6. Cobalt oxide films grown on MgO(001) with an oxygen partial pressure of 5 Pa at different substrate temperatures. By increasing the substrate temperature to 550 °C Co_3O_4 is the preferred phase. All grown films with this oxygen partial pressure are single-phase and single-crystalline. Structural parameters are summarized in Table A.1.

Data availability

Data will be made available on request.

References

[1] A. Ullrich, S. Hohenberger, A. Özden, S. Horn, Synthesis of iron oxide/manganese oxide composite particles and their magnetic properties, J. Nanoparticle Res. 16 (8) (2014) 2580, http://dx.doi.org/10.1007/s11051-014-2580-2.

[2] T. Tepper, F. Ilievski, C.A. Ross, T.R. Zaman, R.J. Ram, S.Y. Sung, B.J.H. Stadler, Magneto-optical properties of iron oxide films, J. Appl. Phys. 93 (10) (2003) 6948–6950, http://dx.doi.org/10.1063/1.1540033.

[3] P. Plate, C. Höhn, U. Bloeck, P. Bogdanoff, S. Fiechter, F.F. Abdi, R. van de Krol, A.C. Bronneberg, On the origin of the OER activity of ultrathin manganese oxide films, ACS Appl. Mater. Interfaces 13 (2) (2021) 2428–2436, http://dx.doi.org/10.1021/acsami.0c15977.

[4] S. Glamsch, H. Karl, Large effect of temperature cycling on the electrical and optical properties of TiO2:H thin films, J. Phys. Chem. C 127 (29) (2023) 14415–14424, http://dx.doi.org/10.1021/acs.jpcc.3c02215.

[5] M. Tadic, D. Nikolic, M. Panjan, G.R. Blake, Magnetic properties of NiO (nickel oxide) nanoparticles: Blocking temperature and Neel temperature, J. Alloy. Compd. 647 (2015) 1061–1068, http://dx.doi.org/10.1016/j.jallcom.2015.06.027.

[6] Y.D. Ji, T.S. Pan, Z. Bi, W.Z. Liang, Y. Zhang, H.Z. Zeng, Q.Y. Wen, H.W. Zhang, C.L. Chen, Q.X. Jia, Y. Lin, Epitaxial growth and metal–insulator transition of vanadium oxide thin films with controllable phases, Appl. Phys. Lett. 101 (7) (2012) 071902, http://dx.doi.org/10.1063/1.4745843.

[7] W. Roth, The magnetic structure of Co_3O_4, J. Phys. Chem. Solids 25 (1) (1964) 1–10, http://dx.doi.org/10.1016/0022-3697(64)90156-8.

[8] R. Saha, S. Ghara, E. Suard, D.H. Jang, K.H. Kim, N.V. Ter-Oganessian, A. Sundaresan, Magnetoelectric effect in simple collinear antiferromagnetic spinels, Phys. Rev. B 94 (1) (2016) 014428, http://dx.doi.org/10.1103/physrevb.94.014428.

[9] P.S. Silinsky, M.S. Seehra, Principal magnetic susceptibilities and uniaxial stress experiments in CoO, Phys. Rev. B 24 (1) (1981) 419–423, http://dx.doi.org/10.1103/physrevb.24.419.

[10] W.L. Roth, Magnetic structures of MnO, FeO, CoO, and NiO, Phys. Rev. 110 (6) (1958) 1333–1341, http://dx.doi.org/10.1103/physrev.110.1333.

[11] P. Dutta, M.S. Seehra, S. Thota, J. Kumar, A comparative study of the magnetic properties of bulk and nanocrystalline Co_3O_4, J. Phys.: Condens. Matter. 20 (1) (2007) 015218, http://dx.doi.org/10.1088/0953-8984/20/01/015218.

[12] D. Bekermann, A. Gasparotto, D. Barreca, C. Maccato, E. Comini, C. Sada, G. Sberveglieri, A. Devi, R.A. Fischer, Co_3O_4/ZnO nanocomposites: From plasma synthesis to gas sensing applications, ACS Appl. Mater. Interfaces 4 (2) (2012) 928–934, http://dx.doi.org/10.1021/am201591w.

[13] Y. Shi, X. Pan, B. Li, M. Zhao, H. Pang, Co_3O_4 and its composites for high-performance Li-ion batteries, Chem. Eng. J. 343 (2018) 427–446, http://dx.doi.org/10.1016/j.cej.2018.03.024.

[14] J. Jiang, J. Liu, R. Ding, X. Ji, Y. Hu, X. Li, A. Hu, F. Wu, Z. Zhu, X. Huang, Direct synthesis of CoO porous nanowire arrays on ti substrate and their application as lithium-ion battery electrodes, J. Phys. Chem. C 114 (2) (2009) 929–932, http://dx.doi.org/10.1021/jp909785g.

[15] R. Xu, J. Wang, Q. Li, G. Sun, E. Wang, S. Li, J. Gu, M. Ju, Porous cobalt oxide (Co_3O_4) nanorods: Facile syntheses, optical property and application in lithium-ion batteries, J. Solid State Chem. 182 (11) (2009) 3177–3182, http://dx.doi.org/10.1016/j.jssc.2009.08.033.

[16] S.K. Meher, G.R. Rao, Ultralayered Co_3O_4 for high-performance supercapacitor applications, J. Phys. Chem. C 115 (31) (2011) 15646–15654, http://dx.doi.org/10.1021/jp201200e.

[17] C. Zheng, C. Cao, Z. Ali, J. Hou, Enhanced electrochemical performance of ball milled CoO for supercapacitor applications, J. Mater. Chem. A 2 (39) (2014) 16467–16473, http://dx.doi.org/10.1039/c4ta02885f.

[18] S. Kandalkar, D. Dhawale, C.-K. Kim, C. Lokhande, Chemical synthesis of cobalt oxide thin film electrode for supercapacitor application, Synth. Met. 160 (11–12) (2010) 1299–1302, http://dx.doi.org/10.1016/j.synthmet.2010.04.003.

[19] N. Ter-Oganessian, Cation-ordered $A'_{1/2}$ $A''_{1/2}$ B_2X_4 magnetic spinels as magneto-electrics, J. Magn. Magn. Mater. 364 (2014) 47–54, http://dx.doi.org/10.1016/j.jmmm.2014.04.019.

[20] J. Cook, M. van der Meer, The optical properties of sputtered Co_3O_4 films, Thin Solid Films 144 (2) (1986) 165–176, http://dx.doi.org/10.1016/0040-6090(86)90409-8.

[21] H. El Aakib, J. Pierson, M. Chaik, C. Samba Vall, H. Ait Dads, A. Narjis, A. Outzourhit, Evolution of the structural, morphological, optical and electrical properties of reactively RF-sputtered cobalt oxide thin films with oxygen pressure, Vacuum 159 (2019) 346–352, http://dx.doi.org/10.1016/j.vacuum.2018.10.065.

[22] E. Barrera, T. Viveros, A. Avila, P. Quintana, M. Morales, N. Batina, Cobalt oxide films grown by a dipping sol–gel process, Thin Solid Films 346 (1–2) (1999) 138–144, http://dx.doi.org/10.1016/s0040-6090(98)01503-x.

[23] K. Shalini, A.U. Mane, S. Shivashankar, M. Rajeswari, S. Choopun, Epitaxial growth of Co_3O_4 films by low temperature, low pressure chemical vapour deposition, J. Cryst. Growth 231 (1–2) (2001) 242–247, http://dx.doi.org/10.1016/s0022-0248(01)01493-2.

[24] A.U. Mane, K. Shalini, A. Wohlfart, A. Devi, S. Shivashankar, Strongly oriented thin films of Co_3O_4 deposited on single-crystal MgO(100) by low-pressure, low-temperature MOCVD, J. Cryst. Growth 240 (1–2) (2002) 157–163, http://dx.doi.org/10.1016/s0022-0248(02)00860-6.

[25] A.U. Mane, S. Shivashankar, MOCVD of cobalt oxide thin films: dependence of growth, microstructure, and optical properties on the source of oxidation, J. Cryst. Growth 254 (3–4) (2003) 368–377, http://dx.doi.org/10.1016/s0022-0248(03)01156-4.

[26] S. Schmid, R. Hausbrand, W. Jaegermann, Cobalt oxide thin film low pressure metal–organic chemical vapor deposition, Thin Solid Films 567 (2014) 8–13, http://dx.doi.org/10.1016/j.tsf.2014.07.029.

[27] C.-S. Cheng, M. Serizawa, H. Sakata, T. Hirayama, Electrical conductivity of Co_3O_4 films prepared by chemical vapour deposition, Mater. Chem. Phys. 53 (3) (1998) 225–230, http://dx.doi.org/10.1016/s0254-0584(98)00044-3.

[28] P. Patil, L. Kadam, C. Lokhande, Preparation and characterization of spray pyrolysed cobalt oxide thin films, Thin Solid Films 272 (1) (1996) 29–32, http://dx.doi.org/10.1016/0040-6090(95)06907-0.

[29] A. Louardi, A. Rmili, F. Ouachtari, A. Bouaoud, B. Elidrissi, H. Erguig, Characterization of cobalt oxide thin films prepared by a facile spray pyrolysis technique using perfume atomizer, J. Alloy. Compd. 509 (37) (2011) 9183–9189, http://dx.doi.org/10.1016/j.jallcom.2011.06.106.

[30] K. Klepper, O. Nilsen, H. Fjellvåg, Epitaxial growth of cobalt oxide by atomic layer deposition, J. Cryst. Growth 307 (2) (2007) 457–465, http://dx.doi.org/10.1016/j.jcrysgro.2007.06.028.

[31] P. Prieto, J.F. Marco, A. Serrano, M. Manson, J. de la Figuera, Highly oriented (111) CoO and Co_3O_4 thin films grown by ion beam sputtering, J. Alloy. Compd. 810 (2019) 151912, http://dx.doi.org/10.1016/j.jallcom.2019.151912.

[32] X.L. Wang, D. Li, T.Y. Cui, P. Kharel, W. Liu, Z.D. Zhang, Magnetic and optical properties of multiferroic $GdMnO_3$ nanoparticles, J. Appl. Phys. 107 (9) (2010) 09B510, http://dx.doi.org/10.1063/1.3358007.

[33] S. Laureti, E. Agostinelli, G. Scavia, G. Varvaro, V.R. Albertini, A. Generosi, B. Paci, A. Mezzi, S. Kaciulis, Effect of oxygen partial pressure on PLD cobalt oxide films, Appl. Surf. Sci. 254 (16) (2008) 5111–5115, http://dx.doi.org/10.1016/j.apsusc.2008.02.055.

[34] A. Matsuda, R. Yamauchi, D. Shiojiri, G. Tan, S. Kaneko, M. Yoshimoto, Room-temperature selective epitaxial growth of CoO (1 1 1) and Co_3O_4 (1 1 1) thin films with atomic steps by pulsed laser deposition, Appl. Surf. Sci. 349 (2015) 78–82, http://dx.doi.org/10.1016/j.apsusc.2015.04.205.

[35] D. Feeler, R.S. Williams, Epitaxial growth of CoO (001) and Co_3O_4 (001) films on MgO (001) by Pulsed Laser deposition, MRS Proc. 341 (1994) 29–34, http://dx.doi.org/10.1557/proc-341-29.

[36] F. Jung, R. Delmdahl, A. Heymann, M. Fischer, H. Karl, Surface evolution of crystalline $SrTiO_3$, $LaAlO_3$ and $Y_3Al_5O_{12}$ targets during pulsed laser ablation, Appl. Phys. A 128 (9) (2022) 750, http://dx.doi.org/10.1007/s00339-022-05805-5.

[37] A. Biswas, C.-H. Yang, R. Ramesh, Y.H. Jeong, Atomically flat single terminated oxide substrate surfaces, Prog. Surf. Sci. 92 (2) (2017) 117–141, http://dx.doi.org/10.1016/j.progsurf.2017.05.001.

[38] S. Wang, B. Zhang, C. Zhao, S. Li, M. Zhang, L. Yan, Valence control of cobalt oxide thin films by annealing atmosphere, Appl. Surf. Sci. 257 (8) (2011) 3358–3362, http://dx.doi.org/10.1016/j.apsusc.2010.11.024.

[39] S. Sakamoto, M. Yoshinaka, K. Hirota, O. Yamaguchi, Fabrication, mechanical properties, and electrical conductivity of Co_3O_4 ceramics, J. Am. Ceram. Soc. 80 (1) (1997) 267–268, http://dx.doi.org/10.1111/j.1151-2916.1997.tb02824.x.

[40] K. Kaneko, Y. Qiao, S. Kaneko, A. Matsuda, Vacuum ultraviolet-enhanced topotactic phase transition and physical properties at the surface of cobalt oxide epitaxial thin films, J. Phys. Chem. C 129 (6) (2025) 3264–3271, http://dx.doi.org/10.1021/acs.jpcc.4c07226.

[41] H.-G. Chen, H.-S. Wang, S.-R. Jian, T.-L. Yeh, J.-Y. Feng, Epitaxial growth of cobalt oxide thin films on sapphire substrates using atmospheric pressure mist chemical vapor deposition, Coat. 13 (11) (2023) 1878, http://dx.doi.org/10.3390/coatings13111878.